# GT2009-59600

## LP TURBINE LAMINAR SEPARATION WITH ACTUATED TRANSITION; DNS, EXPERIMENT AND FLUIDIC OSCILLATOR CFD

**Tobias Ries, Frederick Mohr**
Institut für Luftfahrtantriebe,
Universität Stuttgart
Stuttgart, Germany

**Jenny Baumann, Martin Rose**
Institut für Luftfahrtantriebe,
Universität Stuttgart
Stuttgart, Germany

**Ulrich Rist**
Institut für Aerodynamik
und Gasdynamik,
Universität Stuttgart
Stuttgart, Germany

**Irene Raab**
MTU Aero Engines,
Munich, Germany

**Stephan Staudacher**
Institut für Luftfahrtantriebe,
Universität Stuttgart
Stuttgart, Germany

## ABSTRACT

Laminar separation bubbles form on the back surfaces of aero-engine LP turbine blades. In recent years significant weight and cost reductions and performance improvements have been achieved through a better understanding of the behavior of such separation bubbles. A project is underway at the Universität Stuttgart to study a possible technique to suppress laminar separation bubbles using actuated transition. This paper reports on DNS results with and without actuation for different frequencies, amplitudes and Reynolds numbers, revealing the nature of the transitional process. Early results from an experimental simulation are included. In addition numerical simulations of fluidic oscillators which are capable to provide the required frequencies at a size which would fit into an LP turbine are presented.

## INTRODUCTION

Laminar separation bubbles on the suction sides of aero-engine LP turbine blades became more significant in the recent past due to low Reynolds numbers in small, high flying business jets, increasing lift coefficients and micro gas turbines as used in Unmanned Aerial Vehicles. Low Reynolds numbers of about 50,000 in such turbines in combination with reducing blade numbers and higher turning cause the laminar boundary layer in LP turbines to separate. Many detailed investigations on steady and unsteady blowing in a cascade to reduce such bubbles have been published by Rist, Augustin (2005), Rivir, Sondergaard (2004), Rizetta, Visbal (2005), Volino (2003). The same is true for airfoils at low reynolds numbers (Greenblatt, Wygnanski, 2001), (Seifert, 2002). In several experiments synthetic jets are used to form stream-wise vortices which transport fluid of high kinetic energy into the separation bubble to minimize or even eliminate it. In contrast to that in this study small disturbances with ideally zero net mass flow of distinct frequencies are considered which accelerate the laminar turbulent transition process so that the earlier turbulent boundary layer leads to a reduced separation. In the current study DNS-calculations along with the combination of PIV and hot wires as well as hot film measurements in a low-speed wind tunnel are used. Only DNS-calculations allow the simulation of laminar to turbulent transition. Physically accurate solutions are available without the use of a transition model. This will give a fundamental understanding of these processes in a disturbed LP turbine. The conditions of the LP turbine are simulated in a wind tunnel by a profile on the opposite wall of a flat plate as can be seen in *figure 1*. Such a setup has been used successfully before by Lang (2005). In this study the profile produces a pressure distribution similar to the distribution in an LP turbine. A separation bubble forms on the flat plate which is to be influenced by disturbances, small in amplitude and of a certain frequency brought in shortly before the separation bubble. On the one hand the diffusion at the end of the LP turbine causes the laminar boundary layer to separate, on the other hand small disturbances are amplified, leading finally to transition and a more stable boundary layer. Such small disturbances are present in every real flow, but exciting the right frequency at the beginning of the diffusion can lead to an earlier laminar-turbulent transition. Through this process the separation bubble gets smaller without the need of a high air mass-flow, in contrast to steady blowing. The environment in a real turbine is still very different to the rig. There are high levels of free-stream turbulence, periodic potential and vortical disturbances (Hodson, Dawes, 1998) and noise as well as surface roughness.

These issues must be resolved before engine application is seriously studied. In this paper for the experiment the physical setup is provided, from the numerical side the numerical setup for the DNS-calculations is shown and undisturbed, as well as disturbed DNS-calculations for different Reynolds numbers are presented. Another question is how the required disturbances can be generated on the surface of a turbine stage. First results from a concept using fluidic oscillators are presented.

## NOMENCLATURE

$$A(h,k)=\frac{A_d(h,k)}{U_{d\infty}}$$  [-]  Amplitude of spectral mode *(h,k)*

| | | |
|---|---|---|
| $c_D$ | [-] | Diffusion coefficient |
| $c_p$ | [-] | Pressure coefficient |
| $d_{dh}$ | [m] | Hydraulic nozzle diameter |
| $f_b$ | [-] | Base frequency of the DNS-calculations |

$$f_d=\frac{f\cdot U_{d\infty}}{L_{dDNS}\cdot 2\cdot\pi}$$  [Hz]  Disturbance frequency

| | | |
|---|---|---|
| $h$ | [-] | Index for spectral mode in time |
| $k$ | [-] | Spectral mode index in $z_d$-direction |
| $L_{dgl}, L_{dDNS}$ | [m] | Reference length global / for DNS |
| $M$ | [-] | Oscillator scaling factor |
| $Ma$ | [-] | Mach number |
| $p_{d0}, p_{dthroat}$ | [N/m²] | Static pressure after diffusion / Static pressure throat |
| $Re, Re_{gl}$ | [-] | Reynolds number / Re global |
| $s_{dc}$ | [m] | Chord length |
| $t_d$ | [s] | Time |
| $Tu$ | [-] | Turbulence level |
| $U_{d\infty}$ | [m/s] | Free stream velocity, reference velocity DNS |
| $U_{dgl}$ | [m/s] | Global reference velocity |
| $U_{dn}$ | [m/s] | Area averaged oscillator nozzle velocity |
| $u_d, v_d, w_d$ | [m/s] | Velocity in $x_d, y_d, z_d$-direction |
| $x_d$ | [m] | Stream-wise coordinate |
| $y_d$ | [m] | Wall-normal coordinate |
| $z_d$ | [m] | Span-wise coordinate |
| | | |
| $\alpha_i$ | [-] | Amplification factor |
| $\alpha$ | [-] | Stream-wise wave number |
| $\gamma$ | [-] | Span-wise wave number |
| $\nu_d$ | [m²/s] | Kinematic viscosity |
| $\omega_{dz}$ | [1/s] | Vorticity in $z_d$-direction |
| $\rho_d$ | [kg/m³] | Density |
| $DNS$ | | Direct Numerical Simulation |
| $(h,k)$ | | Fourier modes in frequency, span-wise - wave-number spectrum |
| $^d$ | | Dimensional value |
| $'$ | | Disturbance value |

## TUNNEL GEOMETRY AND NUMERICAL SETUP

In *figure 1* the geometry of the wind tunnel represented by the RANS domain calculated with Ansys CFX can be seen. Shortly after the inlet the fluid is accelerated by reducing the cross section of the channel. On the bottom wall a bleed is adjusted in such a way, that the incoming boundary layer is eliminated. In addition the stagnation point at the beginning of the flat plate on the bottom of the tunnel is positioned at the leading edge. By that a separation bubble potentially causing early transition is avoided. After further acceleration the channel gets wider again simulating deceleration at the end of a turbine blade. Shortly before the beginning of deceleration a
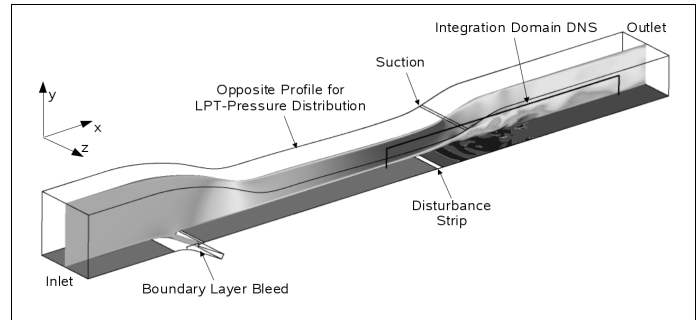
**Figure 1: Model of wind tunnel with DNS-calculation-domain and disturbance strip.**

disturbance strip is located in the RANS simulation as well as in the DNS. At the opposite profile another boundary layer suction is placed to avoid the formation of a separation bubble on the upper profile instead of on the flat plat on the bottom.

Two sorts of numerical investigations were made. RANS calculations, simulating the whole wind tunnel used in the experiment and DNS-calculations simulating the area of the
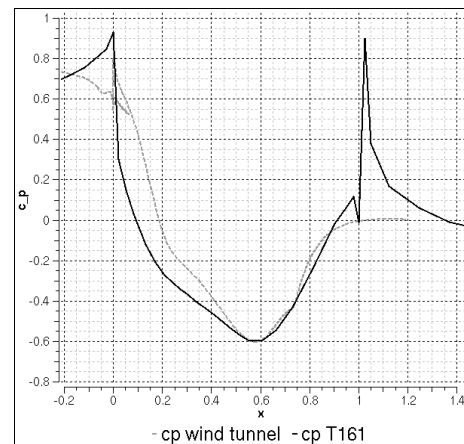
**Figure 2: Cp-distribution comparison T161 - wind tunnel with profile.**

channel where transition is expected and the disturbances are excited. The section where 3D-DNS-calculations are performed is illustrated in *figure 1*. The RANS calculations were used to design the profile which gives the flow field a $c_p$-distribution (*figure 2*) and a diffusion coefficient $c_D$ (1) similar to the distribution in an LP turbine (Ries, Baumann 2009).

$$c_D=\frac{p_{d0}-p_{dthroat}}{\frac{1}{2}\rho_d v_{dthroat}^2}$$ (1)

Copyright © 2009 by ASME

In addition they provide the boundary conditions for the DNS-calculations until experimental data is available. The calculations presented cover two Reynolds numbers (2), 79,164 *(Case Re79k)* and 191,201 *(Case Re191k)*. As usual for turbines the reference velocities are taken at exit. Since the blade surface is represented by a flat plate in this study instead of the true chord the profile surface length $L_{dgl}$, which is about 20-30% larger, is used as reference length for the Reynolds number. Also the $c_p$-distribution of *T161* shown in *figure 2* was transformed to suction side coordinates.

$$Re_{gl} = \frac{U_{dgl} \cdot L_{dgl}}{\nu_d} \qquad (2)$$

## CODE

The code used for the DNS-calculations is *n3d* provided by the IAG (Institut für Aerodynamik und Gasdynamik, Universität Stuttgart). It is the institute's standard tool for accurate simulation of laminar turbulent transition and has proved to be reliable in various applications. It is an unsteady, incompressible 3D-Navier-Stokes-Solver with 4th-order discretization in time, 6th-order in $x$ and $y$ direction and a spectral resolution in $z$. Detailed information is available in Augustin (2005), Kloker, Konzelmann, Fasel (1993), Kloker (1998), Rist, Maucher, Wagner (1996) and Rist, Maucher (2002).
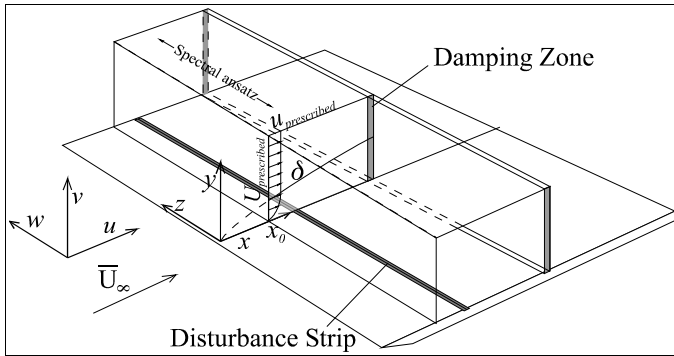


**Figure 3: DNS calculation area scheme.**

## DISCRETIZATION

For the numerical discretization in $x$- and $y$-direction a finite-difference discretization in physical space is used, but the span-wise discretization takes place in Fourier-space. So the span-wise ($z$) direction is solved for a certain frequency. That way the computational effort can be reduced and the important information is still solved for. Resolution in $z$-direction is increased by solving for multiple frequencies, such that the resolved resolution is determined by the span-wise wave lengths and the Nyquist criterion. It is worth noting that an increase in $z$-resolution does not increase the real computational time significantly if analogously more CPUs are taken because the code scales very well. The runtime for a typical unsteady run of cases shown in this paper is 5-10 hours on the NEC SX8 at the high performance computing center of the Universität Stuttgart using one CPU per span-wise mode. The calculation domain is symmetric by definition due to the use of Fourier coefficients. The standard grid for the long integration domain for *Re79k* contains 1250 nodes in $x$-direction, 289 nodes in $y$-direction and for *Re191k* 1170 nodes in $x$-direction and 289 nodes in $y$-direction. A shortened

version with 706 nodes was used for most calculations of *Re79k* to reduce the computational time. In the span-wise direction in this paper two modes were solved for being able to capture the influence of a three-dimensional mode in the breakdown scenario. The reference cases were also calculated with a higher resolution of eight modes in span-wise direction. This was done to make sure that a higher resolution is not absolutely necessary for the calculations presented in this paper. It turned out that the differences did not affect the conclusions.

## INTEGRATION DOMAIN

The integration domain for the DNS-calculations is a rectangular block as can be seen in *figure 1* consisting of an equidistant grid in $x$- and $y$-direction. It starts 360*mm* behind the flat plate leading edge and is 408*mm* long for the initial *Case Re79k* and 419*mm* for *Re191k* calculations. The shortened version of *Re79k* is 237*mm* long. The height in both cases is 30*mm*. To obtain results which are independent of the calculation area, the height of the separation bubble needs to be significantly smaller than the calculation domain. So the top of the calculation domain was set to the maximum extent of the channel, where the upper boundary layer is just not influencing the prescribed velocity boundary layer yet. All $x$ and $y$ coordinates in the diagrams are made non-dimensional with the suction-side surface length with 0.0 representing the blade leading edge and 1.0 the trailing edge. Also all streamline and amplification plots except for *figure 6* and 7 show the same calculation window in real space. The left hand edge of the plots in both cases is 360*mm* behind the flat plate leading edge, at $x$=0.53 and identical with the beginning of the DNS calculation domain. The right hand edge is 563*mm* behind the leading edge at $x$=0.83.

## BOUNDARY CONDITIONS

The rectangular grid for the DNS-calculations requires input for the boundary conditions at the left hand and the top edge. At the left hand edge, a boundary layer velocity profile is prescribed by $u$, $v$ and $\omega_z$. At the top, a $u$-velocity distribution is prescribed (*figure 3*). The lower edge is determined by the no-slip condition, except at the disturbance strip where disturbances are brought into the fluid by exciting the velocity $v$ at the wall sinusoidal in time with the disturbance frequency. In $x$-direction the shape of the disturbance amplitude is determined by a smooth polynomial distribution, in span-wise direction the disturbances are periodic waves with a multiple of the base span-wise wavenumber (Rist, 1999). At the right hand edge the elliptic terms in the equations are eliminated, so that all influences coming from the right side are not taken into account, which is allowed for boundary layer flows. In addition a damping zone is used to eliminate possible reflections of disturbances (Kloker, Konzelmann, Fasel, 1999). The required boundary conditions were taken from the RANS calculations for a first approach.

## DNS – FREQUENCY ANALYSIS

Decelerated flows are sensitive to disturbances of certain frequencies. Once existent, they are amplified exponentially by linear growth mechanisms (Rist, 1998). A stability analysis of the flow field provides the amplification factor $\alpha_i$ for a given
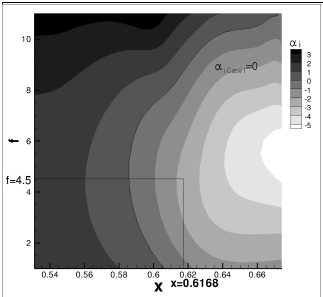
**Figure 4: Stability diagram for *Re79k* providing the amplification factor $\alpha_i$. Negative regions are unstable.**
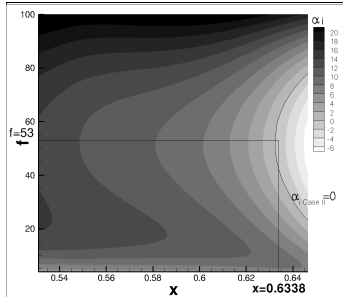


**Figure 5: Stability diagram for *Re191k* providing the amplification factor $\alpha_i$. Negative regions are unstable.**

frequency at a given point in stream-wise direction of a flow field. With this information the optimal point for the disturbance input and the according frequency of maximal amplification can be obtained. The stability solver used for this investigation is *icostab* provided by the IAG. For *Re79k* an optimal dimensionless frequency of *f*=4.5 was found (*figure 4*) whereas for *Re191k* a dimensionless frequency of *f*=53.0 was taken (*figure 5*). The big difference in the values is due to different reference values for the frequency-non-dimensionalisation. $U_{d\infty}=2.59\,m/s$ and $L_{dDNS}=6.1\times10^{-2}m$ was used for *Re79k*, $U_{d\infty}=6.54\,m/s$ and $L_{dDNS}=5.4\times10^{-1}m$ for *Re191k*. Converting these frequencies to dimensional values lead to $f_d$=30.41*Hz* for *Re79k* and $f_d$=102.16*Hz* for *R191k*. The transformation of the frequencies to a real turbine environment results in very high frequencies ranging from about 40*kHz* to 85*kHz* for *Re79k* (*f*=4.5) and 56*kHz* to 108*kHz* for *Re191k* (*f*=53.0), depending on the turbine environment for blades differing from 40*mm* to 70*mm* and inlet velocities from 170*m/s* to 205*m/s*.

## DNS – ANALYSIS

The main object of this project is to investigate the influence of actuation on a laminar separation bubble on an LP turbine blade. Comparisons between actuated and non-actuated separation bubbles can show the effects of actuation on the bubble. In addition, different types of actuation can lead to significant differences in the solutions. Therefore, a matrix of
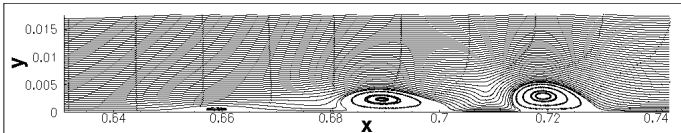


**Figure 6: Instantaneous streamline plot of reference case *Re191k*.**
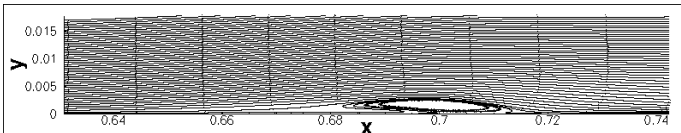


**Figure 7: Time-averaged streamline plot of reference case *Re191k* averaged over one base frequency period.**

different actuation scenarios was set up to obtain more knowledge about the transition mechanisms. For both Reynolds number cases the actuation frequency and amplitude was varied, actuation was switched off, and the position of actuation was changed. In addition the differences between two- and three-dimensional disturbances are presented as well as comparisons between *Re79k* and *Re191k*. In the following figures (e.g. *figure 8*) also amplification curves are plotted which are used to analyse the unsteady simulations. The abscissa represents the stream-wise direction *x*, the ordinate the maximal amplitude in *y* of the Fourier analysed velocity distribution over one actuation period in time. Like the other values also the amplitude of the disturbance velocity is made non-dimensional. This means that at a value of *1.0* the disturbance velocity is equal to the reference velocity $U_{d\infty}$. The results shown in the streamline plots of the following paragraphs are time-averaged over one period of the base frequency $f_B$ and the aspect ratio is stretched in *y*-direction to improve the visualization of the separation bubbles. The real flow with correct aspect ratio would look like in *figure 6* and *7*. In *figure 6* an instantaneous picture of *Re191k* with the eddies rolling downstream is shown. In *figure 7* the same flow just time-averaged over one base frequency period is shown.

## VARIATION OF THE ACTUATION FREQUENCY

As described above, the frequency analysis for *Re79k* in *figure 4* promises highest integral amplification for a frequency of *f*=4.5 and the analysis for *Re191k* for a frequency of *f*=53.0 (*figure 5*). To find out how different frequencies affect the separation bubble, the disturbance frequencies were varied in both cases. For *Re79k* the frequency was changed by 11% to *f*=4.0 and *f*=5.0, whilst for *Re191k* a bigger change of 43% in both directions was applied to *f*=30.0 and *f*=76.0. The reason for this higher variation was to find out if a strong variation has also a strong effect on the bubble size.
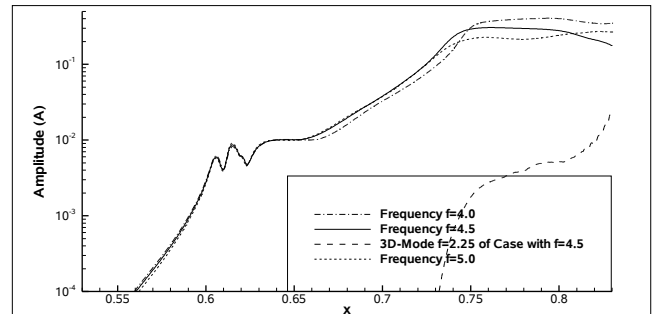


**Figure 8: *Re79k*: Influence of the actuation frequency (*f*=4.0, 4.5, 5.0) with $A=1.0\times10^{-2}$ on the 2D-fundamental modes.**
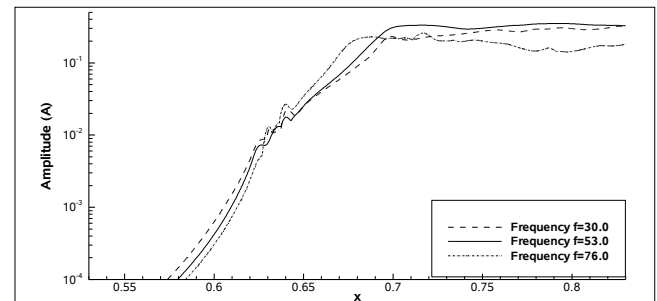


**Figure 9: *Re191k*: Influence of actuation frequency (*f*=30.0, 53.0, 76.0) with $A=1.0\times10^{-2}$ on the 2D-fundamental modes.**

In *figure 8* the amplification curves of the 2D-disturbance-frequencies *f*=4.0, *f*=4.5 and *f*=5.0 are plotted for *Re79k*. In *figure 9* the curves of *f*=30.0, *f*=53.0 and *f*=76.0 are plotted for *Re191k*. In *annex 1.1* it is shown that for *Re79k* the frequency *f*=4.5 seems to be the most suitable for reaching early transition with high amplification which fits to the findings of the stability diagram. The same is true for *Re191k* as can also be seen in *figure 10a-c*. The separation bubble for *f*=30.0 is about 23% longer and for *f*=76.0 about 82% longer in comparison to the one of *f*=53.0. The undisturbed bubble is even 118% longer. So disturbing with *f*=53.0 leads to the most effective reduction in separation bubble size as expected by the stability analysis.

Fig. 10a: Frequency *f*=30.0

Fig. 10b: Frequency *f*=53.0

Fig. 10c: Frequency *f*=76.0


Fig. 11: Non-actuated flow
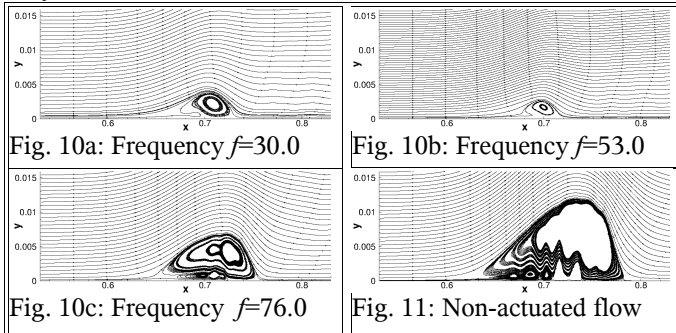
**Figure 10a-c, figure 11: Streamline plots of *Re191k* variating the disturbance frequency for an amplitude of $A = 1.0 \times 10^{-2}$ in comparison with the undisturbed calculation in figure 11.**

In both cases the optimal frequencies from the stability analysis lead to the biggest reduction in separation bubble size. But the big variation of the disturbance frequency in *Re191k* shows also that the effective frequency range is broad. By comparing *figure 10a-c* with the undisturbed calculation in *figure 11,* it can be concluded that frequencies differing by more than 40% compared to the optimal frequency are still able to reduce the size of the separation bubble although with reduced efficiency.

## VARIATION OF THE ACTUATION AMPLITUDE

As described before, the intention of this investigation is to minimize separation bubbles using as little energy as possible. So while a high disturbance amplitude provides the highest probability to minimize a separation bubble, a weak disturbance amplitude is desirable in terms of the energy required. A high amplitude might simply cause bypass-transition whilst the intention is to reach transition by instability modes with low energy input.

For both cases, the amplitude was lowered and increased compared to the reference case by an order of magnitude. The amplitudes were $A = 1.0 \times 10^{-1}$, $A = 1.0 \times 10^{-2}$ (reference case) and $A = 1.0 \times 10^{-3}$.

The results for *Re79k* already show the problem described above. Compared to the reference, the excitation with $A = 1.0 \times 10^{-3}$ is not able to force the flow into strong periodic behavior any more as described in detail in *annex 1.2*. The flow still forms the downstream rolling waves of the disturbed frequency, but they are varying from period to period. Disturbing earlier, as described in the next paragraph, also does not solve that problem. A further reduction of the amplitude in *Re79k* results in uncontrolled behavior. The excited frequency

Figure 12a:
*Re79k*: $A = 1.0 \times 10^{-3}$, *f* = 4.5

Figure 12b:
*Re79k:* $A = 1.0 \times 10^{-2}$, *f* = 4.5

Figure 12c:
*Re79k*: $A = 1.0 \times 10^{-1}$, *f* = 4.5


Figure 13:
*Re79k*: Non-actuated flow
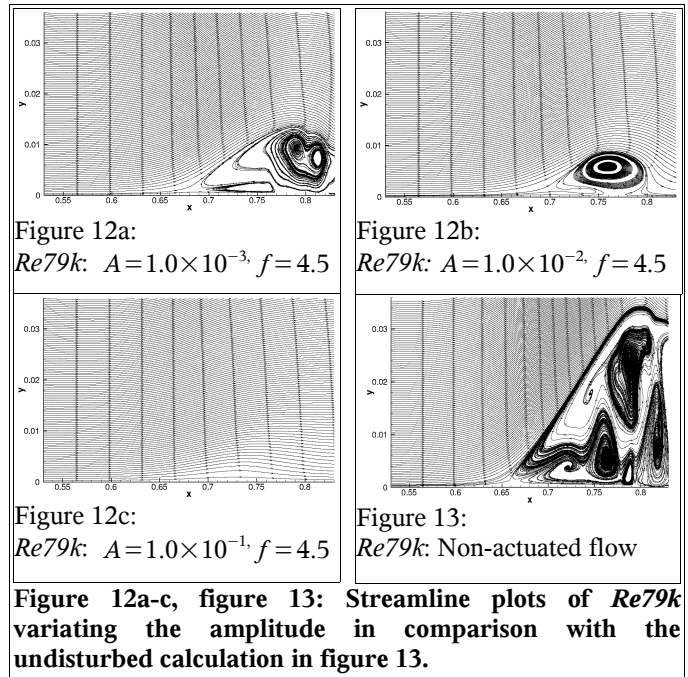
**Figure 12a-c, figure 13: Streamline plots of *Re79k* variating the amplitude in comparison with the undisturbed calculation in figure 13.**

is not able to dominate the flow field any more, different disturbances get excited and lead to uncontrolled, later transition as described in *annex 1.5* and can be seen in the undisturbed case in *figure 13*. On the other side the separation bubble gets continuously smaller with an increase in amplitude. This can be seen in the comparison between the time-averaged flow fields in *figure 12a, b* and *c* for the different amplitudes. For a high disturbance amplitude of $A = 1.0 \times 10^{-1}$ the bubble is gone completely while for $A = 1.0 \times 10^{-3}$ it is about 33% larger. The bubble in the undisturbed case is so unsteady and big, that the accuracy of an increase by about 350% is questionable.

Figure 14a: *Re191k*:
$A = 1.0 \times 10^{-1}$, *f* = 53.0

Figure 14b: *Re191k*:
$A = 1.0 \times 10^{-3}$, *f* = 53.0
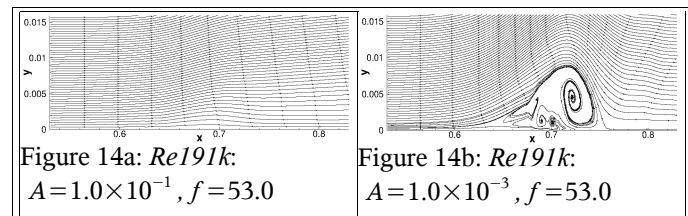
**Figure 14a-b: Amplitude variation for *Re191k*.**

*Re191k* shows similar behavior. For a disturbance with $A = 1.0 \times 10^{-1}$ as can be seen in the average streamline plot in *figure 14a* the bubble is gone completely. In contrast to that using the low amplitude of $A = 1.0 \times 10^{-3}$ already leads to an almost uncontrolled behavior and, with an increase in length by 91%, to a significantly bigger separation bubble as shown in *figure 14b*. Disturbing earlier improves the level of control due to the reasons described in the next paragraph but does not lead to strictly periodic behavior as well. The longest bubble for *Re191k* forms in the undisturbed calculation with about 127% increase compared to the reference case. With regard to both cases it can be concluded that the disturbance amplitude has a lower limit at about $A = 1.0 \times 10^{-3}$, below which the early transition caused by the modal instability does not work any more. Over that limit, the disturbed frequency is coupled in properly and grows quickly up to saturation. There does not

seem to be an apparent upper limit for the actuation, but the growth rate reduces at very high disturbance amplitudes and since minimizing the amount of energy required is desirable, the use of small disturbances would be more efficient.

## VARIATION OF THE ACTUATION POSITION

It could be assumed that disturbing the flow field further upstream might also lead to an earlier transition or a better suppression of the separation bubble. Therefore for both cases the point of disturbance was shifted upstream. For the reference calculation *Re79k* with $A=1.0\times10^{-2}$, the disturbance strip was shifted from $x=0.614$ further upstream to $x=0.561$. As described in detail in *annex 1.3*, disturbing earlier does not lead to an earlier amplification and the size of the separation bubble is almost not affected at all. But it could also be assumed that disturbing earlier for an amplitude of $A=1.0\times10^{-3}$, where the flow is already at the edge to show non-periodic behavior as described above, helps to stabilize the flow. An earlier disturbance for this calculation also answers the question whether an earlier disturbance, which would have more time to lead to transition, could lower the minimal required amplitude for separation control. But also at this lower amplitude, the earlier point of disturbance does not help to stabilize the periodicity of the calculation. This confirms the existence of a minimal required disturbance amplitude for the separation control of about 1% of the reference velocity.

For *Re191k* the results are even more definite. The disturbance input was shifted from $x=0.634$ to $x=0.608$ and $x=0.582$. In *annex 1.3* it is derived in detail that the point of disturbance has no impact on the point of transition. Just disturbing too far downstream like in the reference case can delay transition. This behavior also affects the size of the separation bubble as can be seen in *figure 15a* and *b*. Both early disturbed cases lead to almost identical separation bubbles of the size in *figure 15a*, while the size of the bubble in the reference case in *figure 15b*, where the disturbance lacks of development time, is bigger. For these cases the difference by disturbing earlier leads to a reduction in length by about 27%. For an amplitude of $A=1.0\times10^{-3}$ disturbing earlier at $x=0.608$ leads to a just 55% longer bubble compared with the reference case *Re191k*. This is less than the 91% for the original case with $A=1.0\times10^{-3}$ described above. In addition it has a not strictly periodic, but significantly less random behavior. But this again is just due to disturbing too late for the original calculation. Therefore also at the higher Reynolds number, the position of the disturbance strip is not too important for the solution, as long as the disturbance is not too far downstream.

Both cases allow the point of disturbance to be shifted in stream-wise direction within certain boundaries without having any, or at least without a major impact on the separation bubble. The lower boundary in $x$ is set by moving the disturbance too far upstream. Then the initial disturbance is damped too much before it can get amplified by the diffusion of the flow. The upper boundary for $x$ is to shift the disturbance so far downstream that its location lays in the flow region where earlier disturbed modes are already growing.



Figure 15a: Disturbance at $x$=0.608.

Figure 15b: Disturbance at $x$=0.634 (Reference position)

**Figure 15a-b: Variation of the actuation position for *Re191k*.**
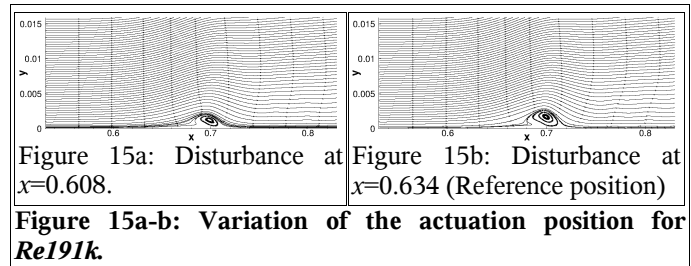
## COMPARISON 2D-3D-DISTURBANCES

Instead of just disturbing with a two-dimensional wave, which has a constant amplitude in span-wise direction, disturbing additionally with a three-dimensional wave could lead to a faster laminar breakdown. Therefore, calculations were made with additional, three-dimensional subharmonic disturbances. of span-wise wave numbers. The time-averaged streamline plots do not show differences in separation bubble sizes. However, there are significant differences in the subharmonic 3D-modes, which are described in detail in *annex 1.4*.

## EXPERIMENTAL SETUP

For the experimental setup an existing wind tunnel was modified. The cross section as well as the length of the test section was therefore fixed. A modular bottom plate was designed to ensure easy changeability of the modules containing actuation or instrumentation respectively. The pressure distribution of a typical separating turbine blade is modeled by a contoured wall opposite a flat plate. Since an optical measurement technique is to be used, the profiled wall and one of the side walls are made of Perspex to enable optical access.

The wind tunnel is sucking air from the test hall. The tunnel velocities are low at about 1*m/s* and changing environmental conditions could heavily influence the behavior of the sucked air. An inlet plenum was designed to cut off these influences. Its cross section is ten times as big as those of the test section. A cut through the plenum and test section as well as the arrangement of the built-in components are shown in *figure 16*. Unlike in most laminar flow test rigs, the inlet of the plenum is a small hole in comparison to the cross section of the tunnel (1). Forcing the air through it and therewith highly increasing the speed of the sucked air is to eliminate environmental disturbances from the flow. Using perforated plates as baffles (2) the fluid is forced to spread over the whole cross section of the plenum. With round shaped (3mm diameter, 50mm length) honeycombs (3) and fabric screens (4) the now low speed flow is made uniform and the strong turbulences produced by the unusual inlet design are damped out, resulting in a turbulence level in the inlet of the test section of *Tu* $\leq$ 0.1%. The contraction from the plenum to the test section cross section is done by a sine-cosine passage (5). It enables a smooth acceleration of the flow and is unlikely to cause separation.

The controlling parameter for the experiments is the Reynolds number *Re* from equation (2). The velocity in the test section depends on the mass flow which is set up by using orifice plates in the downstream pipework. Those orifice plates were designed for a defined total pressure in the test section under the assumption that the flow through them is critical (*Ma*=1.0). Since the mass flow through the orifice plates
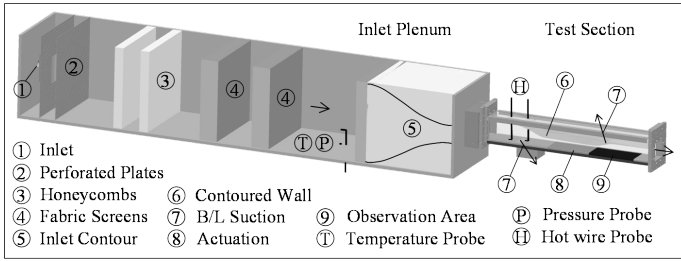
**Figure 16: Schematic of the test rig.**

depends on the total pressure in the test rig, the pressure has to be held constant to assure similar conditions for different test days. The environmental conditions in the test facility can not be held constant but are changing even in a day's time. A cone to enable the size of the inlet to be varied was designed as a solution for this problem. Changing the inlet area and holding constant the mass flow means changing the velocity of the fluid through the inlet. Since the pressure drop scales with the square of the velocity, a defined pressure in the test section can be set up by adjusting the cone depending on the ambient pressure.

## MEASUREMENT TECHNIQUES

The main measurement technique to study the 2D flow field is the Particle Image Velocimetry (PIV). For boundary layer traverses and calculation of the turbulence level $Tu$ hot wire / hot film measurements are taken. To be able to compare the findings with the numerical simulations, $Tu$ should not exceed $1\%$ which can be regarded as a laminar flow field. The turbulence level is calculated from the standard deviations of the measured velocity component $u_d$ and the mean free stream velocity $U_{d\infty}$.

$$T_u = \frac{1}{U_\infty} \cdot \sqrt{\frac{1}{3} \cdot \left( \overline{u'^2_d} + \overline{v'^2_d} + \overline{w'^2_d} \right)}$$

$$\overline{u'^2} = \frac{1}{n-1} \cdot \sum_{i=1}^{n} \left( \overline{u} - u_i \right)^2 \quad (3)$$

In addition also pressure measurements with a Pitot probe are taken. The probe is to sit in front of the test section inlet and is used to control the pressure adjustment by the inlet area variation. The positions of the different probes are marked in *figure 16*.
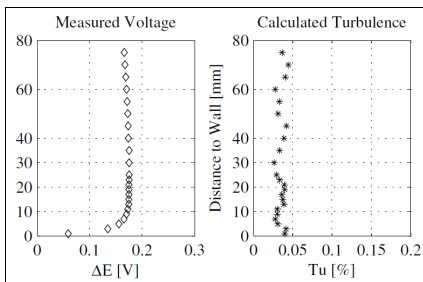


**Figure 17: Voltage distribution and calculated turbulence of the flow 2*cm* back of the stagnation point.**

The experimental results shown in *figure 17* are those of a hot wire traverse in a position 20*mm* downstream of the stagnation point. Since the hot wire probe is not yet calibrated, the measured voltage distribution is displayed rather than the velocity distribution. That does not affect the shape of the boundary layer as the correlation between voltage and velocity is linear for very low velocities ($<5m/s$).

The level of turbulence which is displayed in the diagram on the right hand side does not exceed $0.1\%$. This level of turbulence in the test rig is sufficiently low to avoid free stream disturbances.

## ACTUATION

The actuation is done with a loudspeaker setup where the oscillation of the loudspeakers membrane causes the air in a plenum on top of it to oscillate as well. Controlling this oscillation by the aid of a frequency generator, defined actuation frequencies can be produced.

The current slot is shaped rectangular (width = channel width, length = 0.3*mm*) while the outflow angle is orthogonal to the flow direction. Other geometries and angles are to be investigated as well. For further investigations the implementation of fluidic oscillators into the test rig is planned.

## FLUIDIC OSCILLATORS

The application of instability modes in a real turbine requires a device which is small in size and capable of generating the required frequencies at high temperatures. Therefore a simple, robust device without moving parts is favourable. These boundary conditions are satisfied by fluidic
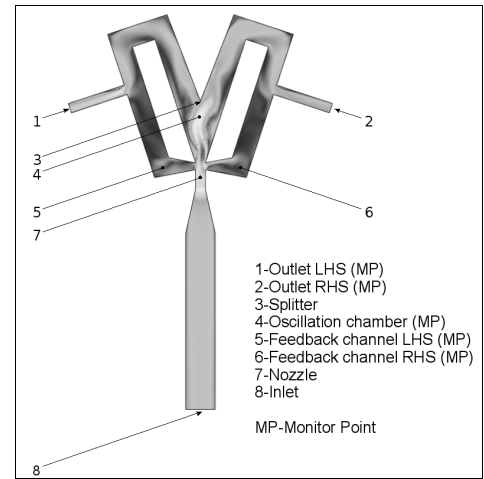


**Figure 18: Schematic of the oscillator.**

oscillators. In *figure 18* the sectional view of the fluidic oscillator investigated in this study is shown. The actuator is based on the Coanda Meter published by Wright, P. H., (1980). Modifications have been made to the geometry in order to gain a two-dimensional cross section that can be extruded to 3D rectangular channels. This reduces efforts in grid generation, the size of the mesh and therefore decreases overall simulation time. The fluid entering the oscillator at the inlet reaches the nozzle and forms a jet in the oscillation chamber. Due to natural or numerical instabilities in the flow the jet tends to one side of the splitter and travels through the corresponding channel. Most of the fluid leaves the oscillator through the outlet, while a part of the fluid is redirected through the feedback channel, where it reaches the nozzle and forces the jet to switch to the other side of the splitter. This switching is repeated periodically, which results in a pulsed outflow of the fluid at a particular frequency.

## MESH AND TIME STEP INDEPENDENCE

The unstructured mesh used for the numerical simulation of the fluidic oscillator is generated with CENTAUR and contains 150,000 nodes and 390,000 elements. To ensure a mesh independent solution, two finer grids were tested with up to more than a million elements. The difference in oscillation frequency was found to be less than 0.5%. In addition, the solution is independent of the time-step if a RMS Courant number smaller than 1.0 is ensured and the RMS-residuals are kept below $1.0 \times 10^{-4}$.

## BOUNDARY CONDITIONS, INITIALIZATION AND SIMULATION

The boundary conditions for the simulation correspond to the flow field characteristics in a low pressure turbine if the oscillator is positioned inside a turbine blade. As inlet boundary conditions static pressure and temperature are used and static pressure at the outlet. Simulations are performed with ANSYS CFX-11 using the Shear-Stress-Transport (SST) turbulence model. The turbulence level at the inlet (*eq. 3*) is set to 5%, the actuator walls to non-slip and adiabatic. The fluid is air as an ideal gas with heat capacity, viscosity and thermal conductivity adjusted to the inlet temperature.

As initial values for the transient simulation, a steady state calculation after 100 iterations is used and continued as a transient calculation until a sufficient number of stable periods occur so that the oscillation frequency can be determined.

## RESULTS

Velocity profiles at different spots in the oscillator as a function of the time-step number are plotted in *figure 19*. The monitor point *Center* is located downstream of the nozzle in front of the splitter. The monitor points *Outlet LHS / Outlet RHS* show the area-averaged velocities at the left and the right outlet, respectively. A stable oscillation appears in the velocity profiles after a starting period necessary for the flow to develop.

The oscillation frequency as a function of Reynolds number is presented in *figure 20*, whereas the oscillation frequency is determined with the area-averaged velocity at one
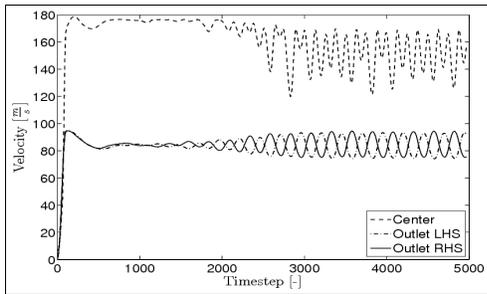
**Figure 19: Velocity over time.**

of the outlets. The Reynolds number (4) is calculated with the area-averaged velocity at the center of the nozzle $U_{dn}$, its hydraulic diameter $d_{dh}$ and the kinematic viscosity.

$$Re_{d_h} = \frac{U_{dn} \cdot d_{dh}}{\nu_d} \qquad (4)$$

The Reynolds number variation is achieved by down-scaling the whole geometry by a scaling factor *M*. The individual points for the different scaling factors can be

approximated by a function of type (5) which may be used to design the oscillator for a special frequency.

$$f = \frac{1}{\ln(Re)} \quad \{Re \in \mathbb{R} : 1.0 < Re < \infty\} \qquad (5)$$
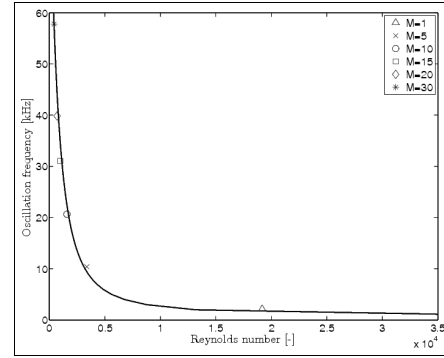
**Figure 20: Oscillation frequency versus Reynolds number.**

## CONCLUSIONS

This paper contains numerical results of DNS-calculations simulating the influence of instability modes on laminar separation bubbles forming in LP turbines at low Reynolds numbers. In addition an overview about research activities at the institute about self-exciting fluidic oscillators which could be used to excite such instability modes in an LP turbine environment is given and the experimental setup used along the DNS-calculations is presented. A low-Reynolds-number flow field in a rectangular wind tunnel with a $c_p$-distribution similar to the one of an LP turbine is used for the investigations. Numerical simulations have been performed with a RANS-solver to obtain a flow field in the channel which provides the boundary conditions for the DNS-calculations before experimental data is available. With these boundary conditions DNS-calculations have been made, covering the area from shortly before the main flow deceleration to after the point of transition for different Reynolds numbers. The DNS-calculations have been performed with and without disturbances. Disturbance frequency, amplitude, position and span-wise wave numbers, as well as disturbance combinations have been changed to evaluate their effect on transition. The influence of these variations on the size of the separation bubble is summarized in *figure 21a-c*. To gather the right range of frequencies which would lead to best amplification and transition, a linear stability solver was used. It was found, that the predictions of the stability solver fitted with the observations in DNS and that there is an optimal disturbance frequency. At a lower frequency fundamental growth starts later, at the higher frequency the maximal amplitude is lower.

Both lead to a bigger separation bubble compared to the optimal disturbance frequency as can be seen in *figure 21a*. It was further found, that the point of initial disturbance input is less important for the transition mechanism, but can delay transition if set too far up- or downstream (*figure 21b*). There is also a critical limit for the excitation amplitude. When it gets below $A = 1 \times 10^{-3}$, the instability mode mechanism does not work any more (*figure 21c*). Additional 3D-disturbances do not have an immediate effect on the bubble size, but may lead to a more robust reattachment. It was also found that separation bubbles of undisturbed calculations were always significantly
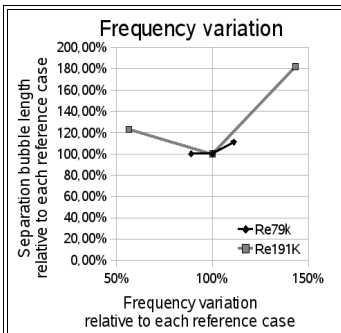
Figure 21a: Frequency variation versus bubble size.
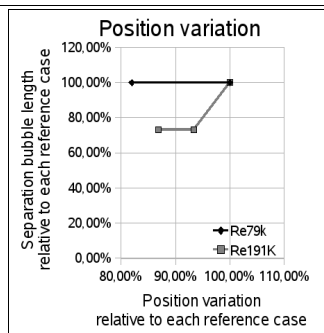
Figure 21b: Position variation versus bubble size.
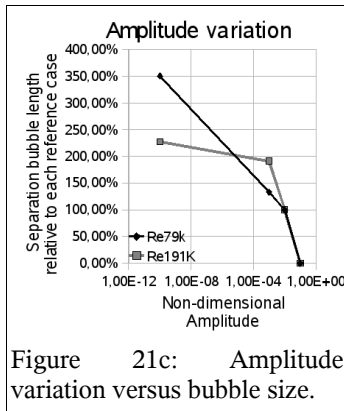
Figure 21c: Amplitude variation versus bubble size.

**Figure 21a,b,c: Effect of frequency, position and amplitude variation on the size of the separation bubble.**

larger compared to according cases with disturbance inputs within the limits described above, as can be seen in *figure 21c* as well. As next steps, the findings have to be reproduced and verified with experimental boundary conditions. In the experimental part, a test rig to study turbine laminar separation with actuation has been prepared. The inlet boundary condition is uniform and has low turbulence intensity ($\leq$0.1%). Early results show the sensitivity of the laminar bubble to actuation. As a possible solution to generate the required frequencies, the use of a fluidic oscillator is discussed. Results of numerical simulations and its behavior depending on the Reynolds number are presented. Although, as described in the introduction, a turbine environment is still very different to the rig, it is concluded that the approach of actuated transition for laminar separation control in LP turbines is promising.

## ACKNOWLEDGMENTS

## REFERENCES

1. K.Augustin, (2005), Zur aktiven Beeinflussung von laminaren Ablöseblasen mittels Grenzschichtstörungen, Dissertation, Institut für Aerodynamik und Gasdynamik, Universität Stuttgart.
2. D.Greenblatt, I.Wygnanski, (2001), Use of Periodic Excitation to Enhance Airfoil Performance at Low Reynolds Numbers, AIAA Journal of Aircraft, Vol. 38, No. 2, 190-192.
3. M.Kloker, U.Konzelmann, H.Fasel, (1993), Outflow boundary conditions for spatial Navier-Stokes numerical simulations of transition boundary layers. AIAA Journal 31 (4), 620-628.
4. M.Kloker, (1998), A robust high-resolution split-type compact FD scheme for spatial direct numerical simulations of boundary layer transition, Applied Scientific Research 59 (4), 353-377.
5. M.Lang, (2005), Experimentelle Untersuchungen zur Transition in einer laminaren Ablöseblase mit Hilfe der Laser-Doppler-Anemometrie und der Particle Image Velocimetry. Dissertation, Universität Stuttgart, Verlag Dr. Hut, München.
6. T.Ries, J.Baumann, LP turbine laminar separation bubble study, flat plate PIV results and DNS-calculations, submitted for 8th European Conference on Turbomachinery (ETC), March 2009, Graz.
7. U.Rist, (1998), Zur Instabilität und Transition in laminaren Ablöseblasen, Habilitationsschrift, Institut für Aerodynamik und Gasdynamik, Universität Stuttgart, Shaker Verlag.
8. U.Rist, K.Augustin, (2005), Control of laminar separation bubbles using instability waves, Proc. ISABE-2005-1041, AIAA Journal 44 (10), October 2006, 2217-2223.
9. U.Rist, H.Fasel, (1995), Direct numerical simulation of controlled transition in a flat-plate boundary layer. J. Fluid Mech. 298, 211-248.
10. H.P.Hodson, W.N.Dawes, (1998), On the interpretation of measured profile losses in unsteady wake – Turbine blade interaction studies.
11. U.Rist, U.Maucher, S.Wagner, (1996), Direct numerical simulation of some fundamental problems related to transition in laminar separation bubbles. In Computational Methods in Applied Sciences '96, ECCOMAS Paris, France, John Wiley & Sons Ltd., 319-325.
12. U.Rist, U.Maucher, (2002), Investigations of time-growing instabilities in laminar separation bubbles. European Journal of Mechanics B/Fluids 21, 495-509.
13. R.B.Rivir, R.Sondergaard, (2004), Control of separation in turbine boundary layers, 2nd AIAA Flow Control Conference 2004, Portland, AIAA 2004-2201.
14. D.P.Rizetta, M.R.Visbal, (2005), Numerical simulation on separation control for transitional highly loaded low-pressure turbines, AIAA Journal, Vol. 43, 1958-1967.
15. A.Seifert, V.Theofilis, R. Joslin, (2002), Issues in Active Flow Control: Theory, Simulation and Experiment, 1st Flow Control Conference, St. Louis, Missouri, June 24-26, 2002, AIAA-2002-3277
16. R.Volino, (2003), Serparation Control on low-pressure turbine airfoils using synthetic vortex generator jets, ASME Turbo Expo 2003,Atlanta, GT2003-38729.
17. P.H.Wright, (1980), The Coanda meter - a fluidic digital gas flow meter, Journal of Physics E Scientific Instruments, Vol. 13, pp. 433-437

**ANNEX 1**

## DETAILED AMPLIFICATION PLOT ANALYSES

### 1.1 VARIATION OF THE ACTUATION FREQUENCY

The amplification curves of the fundamental 2D-disturbance excitation frequencies $f$=4.0, $f$=4.5 and $f$=5.0 for *Re79k* are plotted in *figure 8*. After the disturbance with $A=1.0\times10^{-2}$ at $x$=0.617, there is a short plateau where the mode is not amplified up to $x$=0.653. Then, from $x$= 0.653 on, the modes of $f$=4.5 and $f$=5.0 start to grow from almost exactly the same point with an identical growth rate. This is true up to the critical amplitude of $A=1.0\times10^{-1}$ at $x$=0.725, where the amplitude plot for $f$=4.5 continues to grow with a slightly increased rate up to an amplitude of $A=3.0\times10^{-1}$ at $x$=0.756. The plot for $f$=5.0 reduces in growth rate and reaches its maximum of $A=2.2\times10^{-1}$ at about the same position. This indicates, that due to the higher growth rate at the end, $f$=4.5 is slightly better for providing early transition compared to $f$=5.0. As an example for the typical behavior of the subharmonic 3D-modes, the subharmonic frequency analysis for the case $f$=4.5 with an amplitude of $A=1.0\times10^{-2}$ is plotted in *figure 8*. It does not reach very high amplitudes in the whole flow field and therefore does not have a big influence. The fundamental of $f$=4.0 starts to grow at $x$=0.663, so slightly later than the other two, but with the same growth rate. Like for $f$=4.5, it starts to grow faster at $x$=0.729 and even reaches a higher saturation amplitude of $A=4.0\times10^{-1}$ than for $f$=4.5, but later at $x$=0.788. So the frequency of $f$=4.5 seems to be most suitable for reaching early transition with high amplification which fits to the findings of the stability diagram.

*Re191k* shows a different behavior at the point of disturbance (*figure 9*). In contrast to *Re79k,* fundamental growth starts right at the point of disturbance without delay
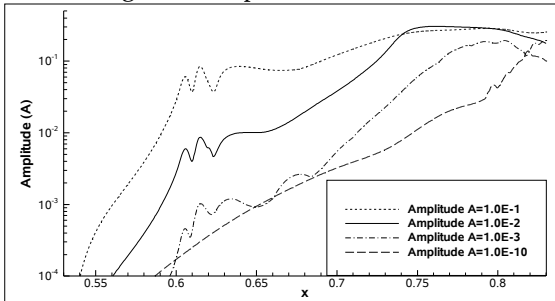


**Figure 22: *Re79k*: Influence of disturbance amplitude on the 2D-fundamental modes for $f$=4.5.**
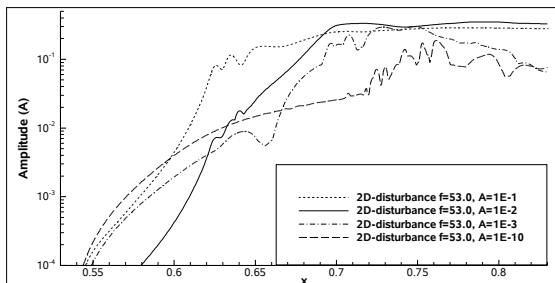


**Figure 23: *Re191k*: Influence of disturbance amplitude on the 2D-fundamental modes for $f$=53.0.**

with high growth rates for every frequency. Unlike the expectation from the stability diagram in *figure 5*, the 2D-mode of $f$=76.0 grows faster than the 2D modes for $f$=30.0 and $f$=53.0 especially from $x$=0.660 on. The 2D mode of $f$=53.0 still reaches the highest absolute amplitude with $A$=0.31, but at about $\Delta x=0.02$ later than the 2D-mode of $f$=76.0. So in the amplification plot the higher frequency seems to have advantages. But as described above, the separation bubble is nevertheless the smallest for $f$=53.0.

### 1.2 VARIATION OF THE ACTUATION AMPLITUDE

An increased disturbance amplitude of $A=1.0\times10^{-1}$ for *Re79k* leads first to a zone of moderate damping, before the excitation starts at $x$=0.670 (*figure 22*). So just a little later than for the reference case, but with a similar behavior. The amplification rate is much lower than in the reference case, nevertheless the critical amplitude of $A=1.0\times10^{-1}$ is already reached after a short distance which is just the result of the high disturbance amplitude of $A=1.0\times10^{-1}$. Saturation, which means no further growth, is not reached earlier than with $A=1.0\times10^{-2}$ due to the lower amplification rate.

Disturbing *Re191k* with a higher amplitude of $A=1.0\times10^{-1}$ leads to a short zone of moderate damping and then, like for *Re79k* from $x$=0.67 on, to growth at a low rate up to saturation (*figure 23*). But with an amplitude of $A=2.6\times10^{-1}$ it is not much higher than the initial disturbance. It is lower than $A=3.3\times10^{-1}$ which is the maximum amplitude of disturbing with $A=1.0\times10^{-2}$, but nevertheless the separation bubble is gone for the high amplitude as can be seen in *figure 14a*.

### 1.3 VARIATION OF THE ACTUATION POSITION

In *figure 24* the amplification plot for the 2D-modes of four calculations of *Re79k* are plotted. The reference calculation of *Re79k* with $A=1.0\times10^{-2}$, the same calculation but with the position of the disturbance strip shifted from x=0.614 further upstream to $x$=0.561, and the same variation for a disturbance amplitude of $A=1.0\times10^{-3}$.
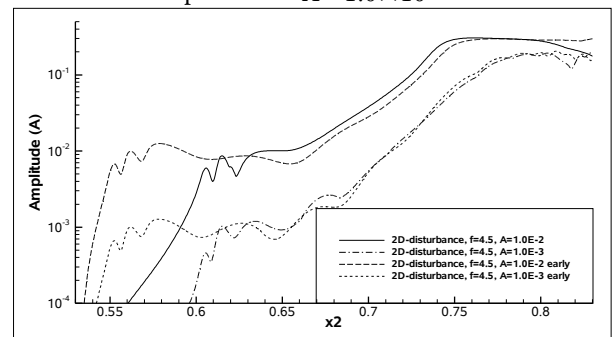


**Figure 24: *Re79k*: Influence of disturbance position on the 2D-fundamental modes for $f$=4.5 and $A=1.0\times10^{-2}$.**

The early actuation for $A=1.0\times10^{-2}$ reaches the same excitation amplitude as the late actuation, but instead of starting to grow, it remains almost on the same level with a small amplitude decay up to the position where the later disturbed case starts to grow. Then it grows with the same amplification as in the later disturbed case from a slightly lower amplitude.

This leads to the fact, that saturation is reached slightly later at $x$=0.774 compared to $x$=0.756 in the reference case. For a disturbance amplitude of $A=1.0\times10^{-3}$ the earlier disturbed fundamental mode again is not amplified up to the point where also the later disturbed fundamental starts to grow.

But also at this lower amplitude, the mode does not begin to grow before $x$=0.653, so that the earlier point of disturbance does not help to establish the periodicity of the calculation. The similarity of the growth process from $x$=0.710 on is even higher. Both curves are almost identical within the fluctuations caused by the not strictly periodic behavior. This confirms the existence of a minimal required disturbance amplitude for the separation control of about 1% of the reference velocity. As
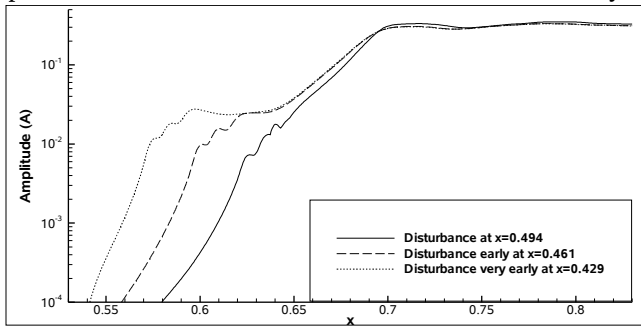


**Figure 25: *Re191k*: Influence of disturbance position on the 2D-fundamental modes for *f*=53.0 and $A=1.0\times10^{-2}$ .**
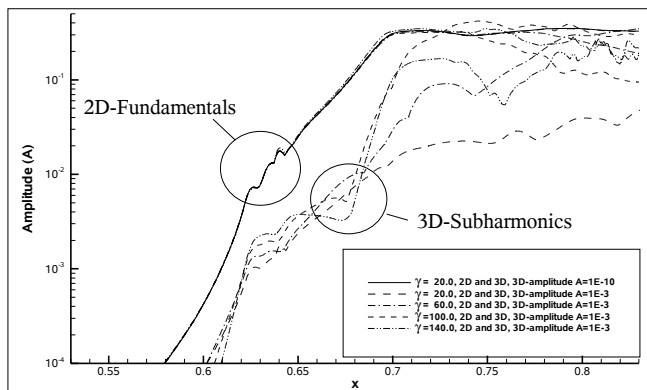


**Figure 26: *Re191k*: Comparison 2D-3D-disturbance with different span-wise wave numbers $\gamma$ .**

shown previously disturbing at the reference position for *Re191k* leads to immediate growth. Moving the disturbance strip further upstream (*figure 25*) from $x$=0.634 to $x$=0.608 leads to a short, non-amplified plateau from $x$=0.615 to $x$=0.647. But from there on the disturbance gets strongly amplified. The growth rate is slightly lower than for the original disturbance, as well as the maximum amplitude. The reason for the slightly different behavior is, that at the original point of disturbance the earlier amplitude already gets amplified. So the original disturbance is disturbed too late to be able to go through the same development. To verify this, another calculation is plotted, where the point of disturbance is moved even further upstream to $x$=0.582. Its fundamental

amplitude stagnates in the beginning as well, and aligns from $x$=0.655 on perfectly with the earlier disturbed case. As described before, this leads to almost identical separation bubbles.

## 1.4 COMPARISON 2D-3D-DISTURBANCES

In *figure 26* the reference calculation of *Re191k* is compared with calculations with additional three-dimensional subharmonic mode disturbances. They have different span-wise wave numbers $\gamma$ , ranging from $\gamma$ =20.0 to $\gamma$ =140.0 with an amplitude of $A=1.0\times10^{-3}$ . The 2D modes are found to be almost unaffected by the presence of the additional subharmonic modes before $x$=0.735. Time-averaged streamline plots also do not show differences in separation bubble sizes. However, there are significant differences in the subharmonic 3D-modes depending on the span-wise wavenumber which also affect the development of the fundamental modes from $x$=0.735 on. The subharmonic mode of $\gamma$ =100.0 seems to be most amplified reaching even higher amplitudes than the fundamental mode and reducing its amplitude from that point on, but as described before, this does not influence the size or position of the separation bubble. Disturbing earlier with an additional subharmonic mode reduces the size of the separation bubble, but just to the extent that already was reached by disturbing earlier without the additional mode. Nevertheless, there is a difference in the time-averaged streamline distribution. With the additional mode, the streamlines behind the bubble continue to run closer to the wall which indicates increased mixing. This might lead to a slightly higher diffusion coefficient or to a more robust design, where a higher diffusion is possible without increasing the size of the separation bubble compared to a single 2D-disturbance.

## 1.5 COMPARISON ACTUATED – NON-ACTUATED FLOW

Amplification plots for the reference calculations and the same calculations without disturbance are plotted in *figure 22* and *figure 23* for both cases. Undisturbed means a very weak disturbance of $A=1.0\times10^{-10}$ which was proven to have no influence on the results. In both cases the fundamental mode of the undisturbed case reaches high amplitudes much later than in the disturbed cases. Whilst in the disturbed calculation of *Re79k* an amplitude of $A=1.0\times10^{-1}$ is already reached at $x$=0.725, the corresponding mode in the undisturbed case does not reach it before $x$=0.824. For case *Re191k* the undisturbed mode does not reach higher values than $A=1.0\times10^{-1}$ before $x$=0.760 and does not grow further whilst the disturbed calculation already reaches it at $x$=0.680 and is saturated at $x$=0.720. Other frequencies might be more dominant in the undisturbed cases, but the streamline plots in *figure 11* and *13* show big separations for both cases. It has to be mentioned, that the separation bubble in the undisturbed calculation of *Re79k* gets so big that it reaches the upper limit of the integration zone, which influences the result. So the accuracy of the value of $x$=0.824 is questionable, but not the fact that transition without disturbance takes place much later.